Digest Journal of Nanomaterials and Biostructures Vol. 18, No. 4, October-December 2023, p.1305-1314

Insight into electronic, magnetic and optical properties of $KMn_xNb_{1-x}O_3$ compound

S. A. Aldaghfag[a], M. Ishfaq[b], S. Saleem[b], M. Yaseen[b,*], M. Zahid[c], M. Shaheen[b]
[a]*Department of Physics, College of Sciences, Princess Nourah bint Abdulrahman University, P. O. Box 84428, Riyadh 11671, Saudi Arabia*
[b]*Spin-Optoelectronics and Ferro-Thermoelectric (SOFT) Materials and Devices Laboratory, Department of Physics, University of Agriculture, Faisalabad 38040, Pakistan*
[c]*Department of Chemistry, University of Agriculture, Faisalabad 38040, Pakistan*

Density functional theory (DFT) based calculations are performed to study the physical features of Mn doped $KNbO_3$. The spin resolved electronic band structure (BS) and density of states (DOS) are investigated that confirmed the half-metallic ferromagnetic (HMFM) character at x=12.5 and 25% Mn concentration. The energy gap of pure $KNbO_3$ is found to majority influenced by Mn-3*d* states which introduces new states in the vicinity of Fermi level. The optical features (dielectric function, absorption coefficient, extinction coefficient, refractive index and optical conductivity) are examined to further reveal the role of Mn doping on the $KNbO_3$ compound for optical devices. Finally in magnetic properties, the total magnetic moment of 2.98 and 3.68 μB which is mainly originated from Mn-3*d* along with weak contribution from K, Nb, and O. Results revealed that $KMn_xNb_{1-x}O_3$ compound is a favorable candidate for optoelectronics and spintronics gadgets applications.

(Received August 10, 2023; Accepted October 25, 2023

Keywords: Half metallic ferromagnetism, First principles calculations, Spintronics, Perovskite oxides

1. Introduction

Complex metal oxides have long piqued the curiosity of researchers across a variety of fields owing to the fact that they can display intriguing physical features ranging from 'simple' magnetism and electronic states to 'complex' collective behavior like magnetoresistance and ferroelectricity [1]. As a typical illustration of collective behavior, magnetic semiconductors are substances that concurrently utilize the electrons' spin and charge to display magnetism with semiconducting states which is prerequisite for the development of spintronic devices [2]. Robust ferromagnetism with 100% spin-polarized asymmetric electronic states, having metallic nature in one spin channel and semiconducting state in other spin channel usually termed as half metallic ferromagnetism (HMFM) display even more complex collective behavior than magnetic semiconductors [3]. HMFM is a complex phenomenon, materials exhibiting this behavior can be developed by doping the transition metal in a wide bandgap semiconductor. The combined effect of metallicity and semiconducting states along with robust magnetism in a HMFM material can be viable option for the development of futuristic spintronic devices. Quest for development of HMFM material has attracted researcher's attention and evolved as separate class of materials. A significant role in the field of material design is played by the perovskite family, one of the most prominent and resilient structural types in complex metal oxides. Perovskites are promising options for use in the future since it is simple to adjust the size and direction of metal-oxygen coupling contacts by changing the contents of unit cells and crystallographic structures.

With a general formula of ABO_3 (where A and B are any suitable cations), these materials are reported as environment friendly and have developed as replacement for lead-containing ferroelectric materials because of their prominent features including the nonlinear-optical [4],

* Corresponding author: myaseen_taha@yahoo.com
https://doi.org/10.15251/DJNB.2023.184.1305

piezoelectric [5], photocatalytic processes [6], photorefractive [7], pyroelectric [8], and optoelectronic [9]. Their structures possess a unique nature with its unusual energy bands and are being utilized in various gadgets to speed up the data processing via increasing integration-circuit's density eventually leading to lower energy usage [10]. HMFM behavior has been experienced in various perovskites owing to their distinctive electronic behavior. Because of this exceptional behavior, such type of material is considered as highly promising candidate for great technological implications, specially are being extensively utilized in the field of spintronics. In the past, most broadly studied transition metals doped materials have shown room temperature ferroelectricity [11, 12]. The transition metal ion shows different properties like ferroelectricity, superconductivity, magnetism and thermoelectricity [13]. Significant magneto-electric effect is observed experimentally at a room temperature in Co-doped $KNbO_3$ compound [14]. The perovskite oxides had been doped with various transition metals targeting to attain new electromagnetic features [15].

Being specific, $KNbO_3$ (KNO) is the one of the most important materials in perovskite family and plenty of strategies are proposed to tune its physical characteristics [16]. Recently, evaluation of phase transitions, remnant polarization, and dielectric susceptibility characteristics in KNO are theoretically reported [17]. It is noticed that Ba/Ni doped KNO compound exhibited exceptional decrease in band-gap from 3.30 to 1.18 eV, with major participation of Ni-3*d* electron, and with variation of electromagnetic properties [18]. Okoye et al. explored the optoelectronic characteristics of paraelectric (cubic) phase KNO and also revealed its structural transitions [19]. Wang et al. investigated pressure induced electronic properties of KNO to determine the charge transferring between atoms from theoretical and experimental approach [20]. The pressure induced phase transition implies the importance of KNO based ferroelectric materials for futuristic applications [21]. Also, it was found that the Cu-doped KNO shows metallic nature if concentration is increased to a substantial level, which is originated owing to the hybridization among Cu-*3d* and O-*2p* states [22].

In this study, the magneto-optoelectronic characteristics of KNO are tailored by Mn substitution at concentration 12.5 and 25% by employing GGA method within DFT. First, electronic properties of doped systems are studied by computing band structures and total and partial DOS. Then we presented frequency dependent optical parameters. Our computed outcomes are obliging to apply this material in various spintronics and optoelectronic gadgets.

2. Computational details

Computations of $KNbO_3$ are done by employing DFT based full-potential linearized augmented plane wave (FP-LAPW) method as coded in WIEN2k [23]. The FP-LAPW method consists of two parts for crystal unit cell; one is interstitial region and the other is muffin tin (MT) zone. The potential in interstitial zone is expanded in term of plane wave orbital and the potential in both regions is shown below:

$$V(r) = \begin{cases} \sum_{LM} V_{LM}(r) Y_{LM}(\hat{r}) & inside\ sphere \\ \sum_{K} V_K e^{iK.r} & outside\ sphere \end{cases} \quad (1)$$

The grid of 1000 Monkhorst-pack meshes in the first Brillion zone is used to compute the properties. The atomic radii conversions are done by G_{max} factor which is taken as 14 [24]. The K and Nb atoms are situated at (0, 0, 0), (0.5, 0.5, 0.5), correspondingly whereas O atoms are centered at (0, 0.5, 0.5), (0.5, 0, 0.5) and (0.5, 0.5, 0) in $KNbO_3$. The compound is found to be nonmagnetic in nature and it is stable in cubic structure with Pm-3m (221) space group. The muffin tin radii (R_{MT}) for K, Nb, O, and Mn are 2.80, 2.15, 0.6, and 2.43 (Å) respectively.

The lattice parameters values are calculated as 4.057 Å for KNO which is much comparable to the theoretical results of Okoye et al [19]. The electronic configuration of Potassium, Niobium, Oxygen, Cobalt and for Manganese is [Ar]$4s^1$, [Kr] $4d^4 5s^1$, [He] $2p^4 2s^2$, [Ar] $3d^7 4s^2$ and [Ar] $3d^5 4s^2$, respectively.

3. Results and discussions

3.1. Electronic properties

The calculated spin-dependent BS of $KMn_xNb_{1-x}O_3$ at (x=12.5% and 25%) are given in Figs. 1 and 2. Electronic plots illustrate the spin up/down electronic BS of the Mn doped $KNbO_3$ besides with high symmetrical directions in a Brillion zone. The Mn doped $KNbO_3$ compound provides varying band plot of energy. In a spin down version, the overlapping of valence bands maxima (VBM) and the conduction band minima (CBM) has been detected, that specifies conducting behavior of a Mn-doped $KNbO_3$ compound. Calculated band structure of $KMn_xNb_{1-x}O_3$ (x=12.5% and 25%) displays half-metallic behavior, whose spin down version behaves like a metallic compound with a large number of the partially filled states beyond Fermi-level and spin-up being a semiconductor. The calculated value of energy gap are 0.81 and 0.88 eV (direct band gap) for 12.5% and 25% doping, respectively while pure $KNbO_3$ gives 2.3 eV band gap [25].

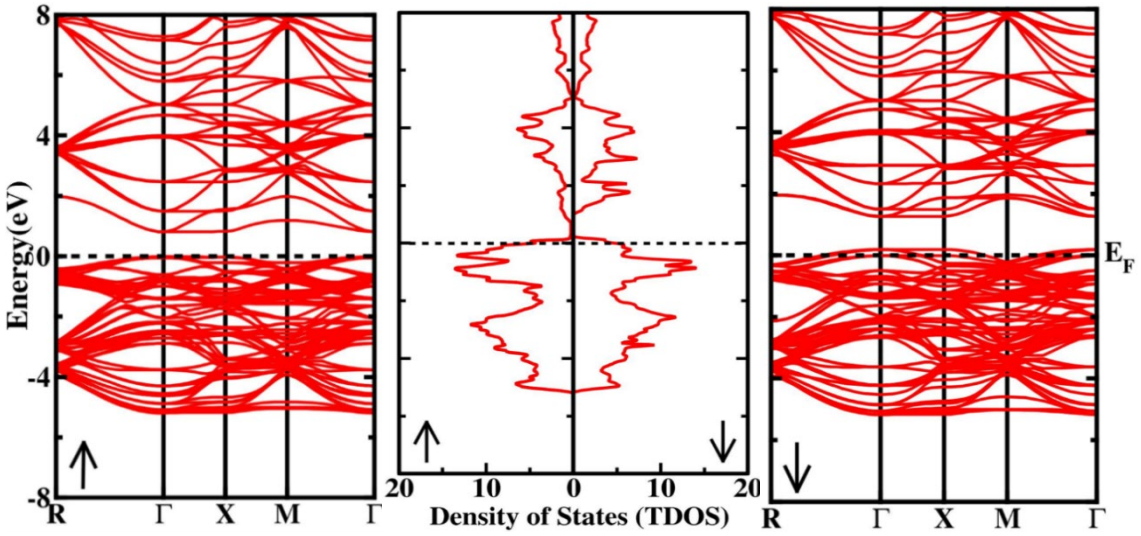

Fig. 1. BS of $KMn_{0.125}Nb_{0.87.5}O_3$ for both spins.

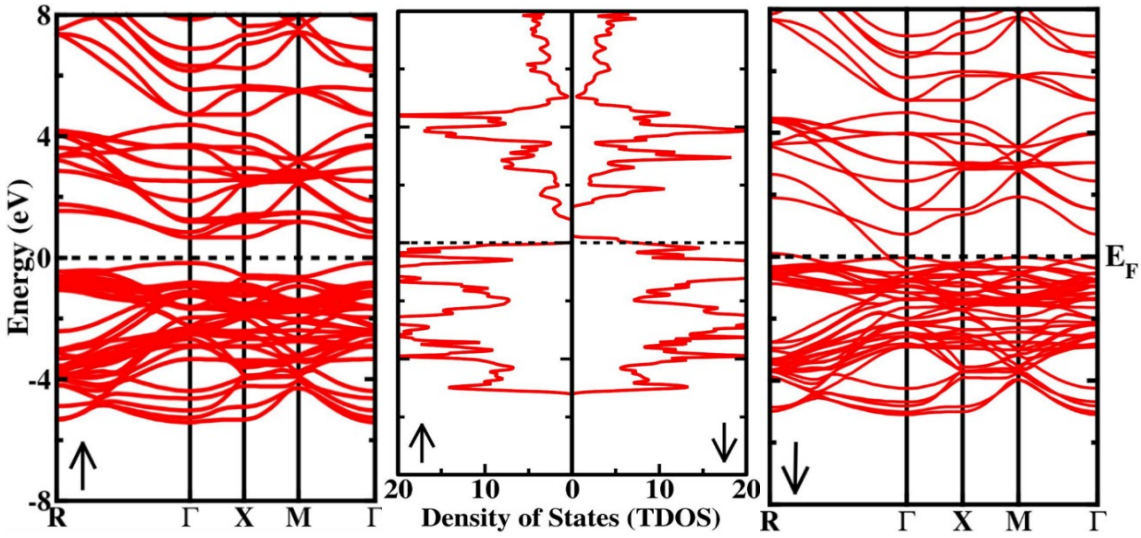

Fig. 2. BS of $KMn_{0.25}Nb_{0.75}O_3$ for both spins.

To examine the source of impurity energy-levels of the $KNb_{1-x}Mn_xO_3$ (x=12.5 and 25%) compounds, total and partial DOS are calculated. TDOS of Mn-doped $KNbO_3$, for spin up/dn version are specified in Fig. 3(a, b). After doping of transition metals (TM), the change in a DOS arises [26] which depends on the orientation of the spins, also leads to particular new states nearby the Fermi level (E_F) by altering electronic properties of a pure $KNbO_3$ compounds. The DOS offers a complete statistic about occupancy of various electronic states of varied energy ranges, and respective valence and conduction band energy levels [27]. It is also observed that the states of the Mn atoms play a very significant role in a both valence bands (VB) and conduction band (CB). To understand the electronic BS, the calculations of total and partial DOS are crucial which are displayed in Fig. 3(a-d). In total density of states, when 12.5% Nb is substituted by Mn, the metallic behavior is perceived in the spin-down version by overlapping of the VB and CB in Fermi region, and a considerable band-gap is detected in majority spin version, as depicted in Figs. 1 and 2. For the sake of relationship among a pure and doped $KNbO_3$ compound, partial DOS of Mn-doped $KNbO_3$ system are schemed, that demonstrate an important difference in a VB and CB [28], before and after doping. The Nb-4*d* is mostly contributing atom in a spectrum of partial density of states, and contribution of Mn-3*d* is also important because of doping of the Mn in $KNbO_3$ compound, however, a new peak is observed above E_F as demonstrated in Fig. 4(a-d), while K-*s* shows small contribution as compared to Nb-4*d*, and the Mn-3*d*. In Mn-doped $KNbO_3$ at x=12.5% shows half metallic behavior because of hybridization of 3*d*-state of the TM, Nb-d-state and d-*eg* state of Mn (see Fig. 3c). At 25% concentration, the energy gap observed in spin-dn version because of hybridization of Mn-3*d* transition metals, and O-2*p* state (see Fig. 3d).

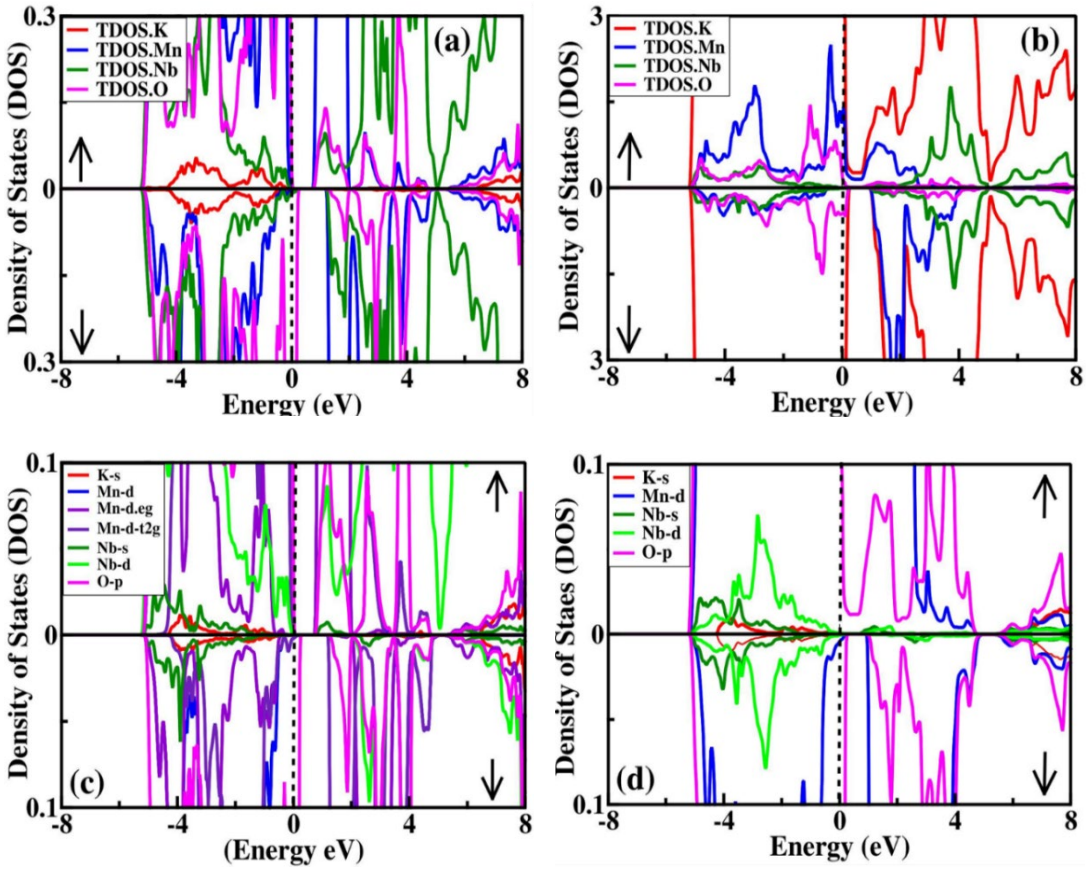

Fig. 3. (a-b) total, and (c-d) partial DOS plots of $KMn_{0.125}Nb_{0.87.5}O_3$ and $KMn_{0.25}Nb_{0.75}O_3$.

3.2. Optical properties

In optoelectronics, optical features of a compound expose its suitability for technological implications [29]. The dielectric function ϵ(ω) is used to represent the system's linear response to electromagnetic (EM) radiation which is defined as:

$$\varepsilon(\omega) = \varepsilon_1(\omega) + i\varepsilon_2(\omega) \tag{2}$$

The imaginary $\epsilon_2(\omega)$ and real $\epsilon_1(\omega)$ part of the ϵ(ω) show optical behavior of the materials owing to absorption and dispersion of the impinging frequencies, respectively. At all energies of the photons E = ħω, the Ehrenreich and Cohen formalisms have been employed to characterize material's response to the incident light [30]. The $\epsilon_2(\omega)$ can be attained by computing momentum's matrix element associated via VB and CB states [31]. It was computed by using following relation.

$$\varepsilon_2(\omega) = \frac{e^2\hbar}{\pi m^2\omega^2}\sum_{vc}\int |n, n'(k,q)|^2\,\delta\left[\omega_{n,\acute{n}}(k) - \omega\right] d^3k \tag{3}$$

The $\epsilon_1(\omega)$ can be derived from $\epsilon_2(\omega)$ via Kramers-Kronig transformations.

$$\varepsilon_1(\omega) = 1 + \frac{2}{\pi}p\int_0^{\theta}\frac{\omega'\varepsilon_2(\omega')}{\omega'^2-\omega^2}d\omega' \tag{4}$$

The $\epsilon_1(\omega)$ of the ϵ(ω) is explained in Fig. 4(a) for Mn doped $KNbO_3$ at 12.5 and 25% concentration within the span of 0-14 eV. The values of static dielectric $\epsilon_1(0)$ of $K_{1-x}Mn_xNbO_3$ at x=12.5 and 25% are 14.96, 19.22, respectively. The $\epsilon_1(\omega)$ values starts to fluctuate down via upsurge of energy owing to change in transition rate (see Fig. 4a). At certain energies limit (4.3-5.6 eV), $\epsilon_1(\omega)$ decreases that it even become less than zero and show negative sign. The negative ϵ_1 (ω) represent that radiations are impeded to propagate and are reflected back, signifying the metallic nature and then increases after 6 eV and become stable. The inverse relation exists among static real part and energy band gap (E_g) according to Penn's law [32]. The expression of Penn's law can be signified as $\epsilon_1(0) \approx 1 + (\hbar\omega_p / Eg)^2$ that exhibits low E_g, leads to higher $\epsilon_1(0)$ values.

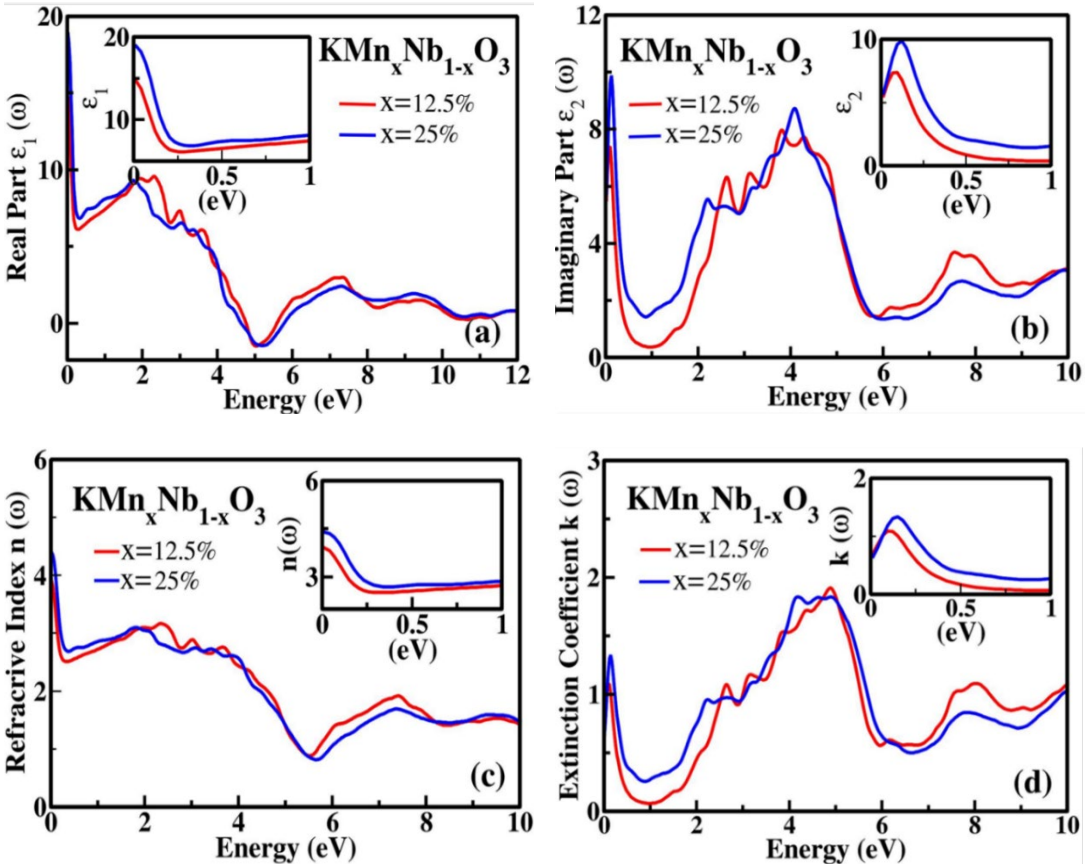

Fig. 4. (a) $\epsilon_1(\omega)$, (b) $\epsilon_2(\omega)$, (c) $n(\omega)$ and (d) $k(\omega)$ for $KMn_xNb_{1-x}O_3$.

The polarization of an incident photon is lower and absorption is higher at prominent peak of $\epsilon_2(\omega)$. The prominent peak of $\epsilon_2(\omega)$, appears at 0.126 at 25% concentration, as represented in Fig. 4b. The values of static dielectric $\epsilon_2(0)$ of $KMn_xNb_{1-x}O_3$ at x=12.5, 25% are 7.66 and 8.94, respectively. In the $\epsilon_2(\omega)$, doping of the TM impurity decreases the sharpness of peaks, but upsurges width of absorption zone simultaneously associated via pristine $KNbO_3$ system since material's absorption is high for higher values of the $\epsilon_2(\omega)$. The refractive index $n(\omega)$ exhibit amount of light passed through a material. The extinction coefficient $k(\omega)$ and $n(\omega)$ demonstrate a comparable trend to that of $\epsilon_1(\omega)$ and $\epsilon_2(\omega)$ and connected with each other by relation $\epsilon_2(\omega) = 2nk$, and $\epsilon_1(\omega) = n^2 - k^2$ [33]. The values of static $n(\omega)$ for $KMn_xNb_{1-x}O_3$ at x=12.5 and 25% are 3.93, 4.43, correspondingly as illustrated in Fig. 4c.In a range from 0-10 eV, $n(\omega)$ is decreased however after 10 electron volt, it gives constant values. The refractive index can be computed from the following formulation:

$$n(\omega) = \left(\frac{\left[\varepsilon_1^2(\omega) + \varepsilon_2^2(\omega)\right]^{\frac{1}{2}} + \varepsilon_1(\omega)}{2} \right)^{\frac{1}{2}} \tag{5}$$

The static $\epsilon_1(\omega)$ and $n(\omega)$ are associated via the relation: $n(0) = \sqrt{\epsilon(0)}$. The $k(\omega)$ has same behavior as $\epsilon_2(\omega)$ also defines the degree of attenuation of incident light in $KMn_xNb_{1-x}O_3$ (x=12.5% and 25%). The prominent peaks of k (ω) appear at 0.05 eV for both 12.5 and 25% concentrations (see Fig. 4d). Afterwards, the $k(\omega)$ values decrease sharply at around 1.0 eV followed by a sudden fluctuated increase till 5.0 eV exhibiting the strong absorptive behavior at this point. Above, 5.0 eV, the $k(\omega)$ values modestly decrease up to 10.0 eV.

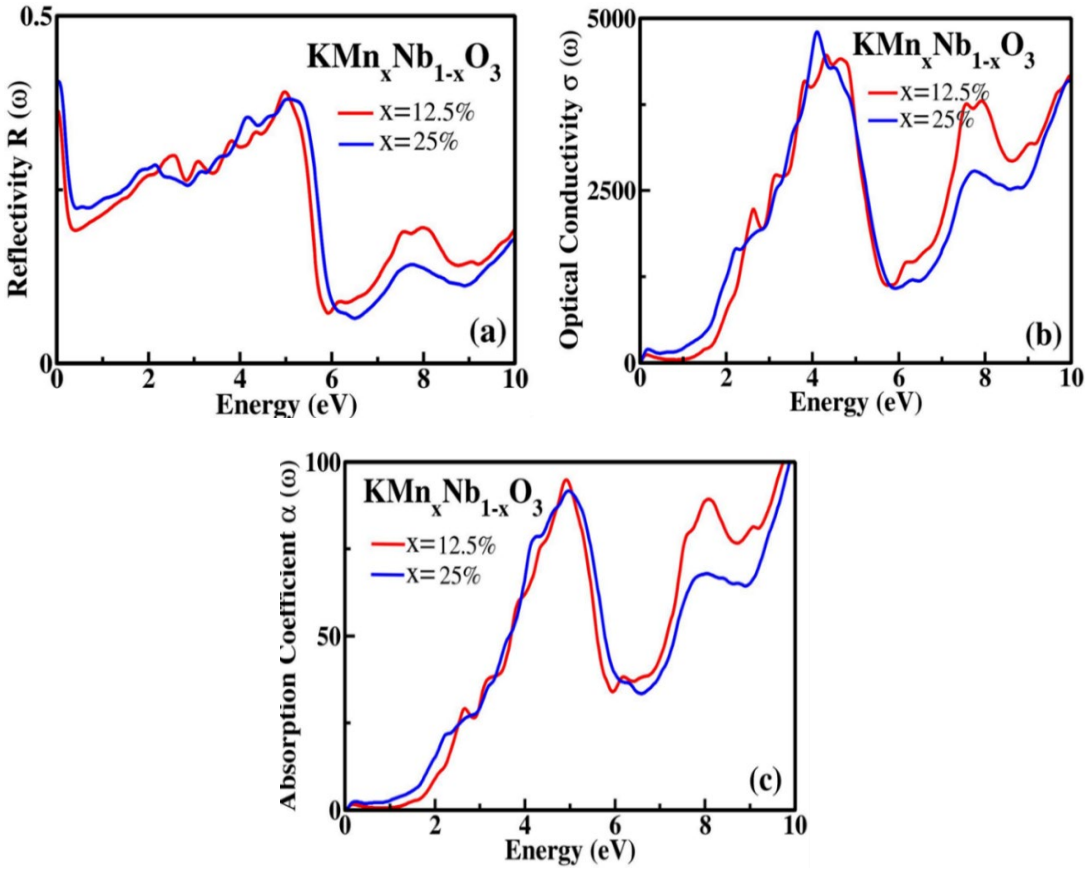

Fig. 5. (a) R(ω), (b) σ(ω) and (c) α(ω)for $KMn_xNb_{1-x}O_3$.

The absorption coefficients α(ω) define the light absorbance capability of the compound. The α(ω) of $KMn_xNb_{1-x}O_3$ compound initiates to upsurge from 0 eV, and then after fluctuations, the highest absorption peaks are attained at 4.4 -5.9 eV for $KMn_xNb_{1-x}O_3$ in visible to ultra-violet (UV) light energy range as depicted in Fig. 5a. So, the resultant material is appropriate for optoelectronic devices. It can be examined by the expression:

$$I(\omega) = \frac{4\pi}{\lambda}\left(\frac{\left[\varepsilon_1^2(\omega)+\varepsilon_2^2(\omega)\right]^{\frac{1}{2}}+\varepsilon_1(\omega)}{2}\right)^{\frac{1}{2}} \quad (6)$$

The σ(ω) states the bond breaking in material caused by incident EM wave. It contents the Maxwell's relation of EM wave to transform photon energy into electrical energy [32]. The designed σ(ω) spectrum is illustrated in figure 5(b).The σ(ω) is lowest for pristine $KNbO_3$ compound, however after doping of the transition metal, like $KMn_xNb_{1-x}O_3$ (x= 12.5% and 25%), value of the σ(ω) increases. σ(ω) of the material is produced by transportation of electrons because of photons radiations. Maximum values of the σ(ω) prove the capability of the Mn doped $KNbO_3$ compound for photovoltaic applications.

Reflectivity R(ω) of $KMn_xNb_{1-x}O_3$ (x= 12.5% and 25%) system is frequency dependent, and analyze surface behavior. The surface behavior of Mn doped $KNbO_3$ compound is analyzed via reflection of light. R(ω) decreases from 0 eV and second maximum R(ω) value is obtained at a precise energy where material show low absorption (see Fig. 5c). Various intensity peaks exhibit the photon's reflection with altered angles of incident from material's surface. Static reflectivity R(0) for $KMn_xNb_{1-x}O_3$ (x= 12.5% and 25%) compound are 0.36 and 0.40, respectively, as shown in Fig. 5(c). Reflectivity of these compounds increases with increasing system's metallicity and then approaches to its highest value at a lower $\epsilon_1(\omega)$.

3.3. Magnetic properties

To investigate magnetism of compound, we computed total and localized magnetic moment values as tabulated in Table 1. The calculated total magnetic moments for $KMn_xNb_{1-x}O_3$ (x= 12.5% and 25%) compound are 2.9836 and 3.68853 μB, respectively (see Table 1). The partial magnetic moments of Mn are 2.64344, 2.61061 μB for $KMn_{0.125}Nb_{0.87}O_3$ and $KMn_{0.25}Mn_{0.75}O_3$, respectively. The total magnetic moment materialized because of large participation of the 3*d* orbit of dopant (Mn) atom and small participation of K, Nb, and O. Many of the perovskite materials display magnetic ordering, and large range of magnetic structures as a result can be found [34, 35].

Table 1. Calculated total, interstitial magnetic and the partial moments in unit (μB) for $KMn_xNb_{1-x}O_3$ compound.

Compound	Total	Interstitial	K	Mn	Nb	O
$KMn_{0.125}Nb_{0.875}O_3$	2.9836	0.24859	-0.00007	2.64344	-0.01076	0.10248
$KMn_{0.25}Mn_{0.75}O_3$	3.68853	0.18221	0.00016	2.61061	-0.00875	0.09043

4. Conclusion

The electronic, magnetic and optical features of $KMn_xNb_{1-x}O_3$ are computed by density functional theory which is implemented in WIEN2k software. HMFM has been showed via Mn-doping in $KNbO_3$ at different concentration. The energy gaps of pure $KNbO_3$ are found to decrease by doping concentration with transition metals. The investigated magnetic features of the Mn doped $KNbO_3$ compound provides magnetic moment with major contribution of Mn. $KMn_{0.125}Nb_{0.87.5}O_3$ and $KMn_{0.25}Nb_{0.75}O_3$ illustrate the total μB of 2.9836 and 3.68853 μ_B, respectively. Furthermore, maximum n(ω) and α(ω) of studied compound in the visible to UV zone suggest that the $KMn_xNb_{1-x}O_3$ could be suitable for optoelectronic gadgets. Results showed that the Mn doped $KNbO_3$ material is appropriate for optoelectronics and spintronics applications.

Acknowledgements

The authors express their gratitude to Princess Nourah bint Abdulrahman University Researchers Supporting Project number (PNURSP2023R81), Princess Nourah bint Abdulrahman University, Riyadh, Saudi Arabia.

References

[1] Liang, Y. and Shao, G., RSC advances, 9(13), 7551-7559 (2019); https://doi.org/10.1039/C9RA00289H
[2] Jin, L., Ni, D., Gui, X., Straus, D.B., Zhang, Q. and Cava, R.J., Journal of Materials Chemistry C, 10(8), 3232-3240 (2022); https://doi.org/10.1039/D1TC05585B
[3] Ishfaq, M., Yaseen, M., Al-Harbi, F.F. and Butt, M.K., Physica B: Condensed Matter, 415025 (2023); https://doi.org/10.1016/j.physb.2023.415025
[4] Vlazan, P., Sfirloaga, P., Poienar, M., and Stoia, M., Materials Today: Proceedings 4(7), 7018-7024 (2017); https://doi.org/10.1016/j.matpr.2017.07.032.
[5] Yang, D., Wang, Y., Li, L., Yao, M., Zhang, W., Gu, H., Zhang, S., Fan, M., Sewvandi, G. A., and Hu, D. Inorganic Chemistry 60(1), 97-107 (2020); https://pubs.acs.org/doi/10.1021/acs.inorgchem.0c02409.
[6] Xu, Y. Q., Wu, S. Y., Ding, C. C., Wu, L. N., and Zhang, G. J. Chemical Physics, 504, 66-71 (2018); https://doi.org/10.1016/j.chemphys.2018.03.007.
[7] Rupa, S. S., Haque, Y., and Das, S. K., Scientific Research Journal 2(7), 2201-1796 (2014);

[8] Matsumoto, K., Hiruma, Y., Nagata, H. and Takenaka, T., 2008. Ceramics International, 34(4), pp.787-791. https://doi.org/10.1016/j.ceramint.2007.09.026
[9] Faridi, M. A., Tariq, S., Jamil, M. I., Batool, A., Nadeem, S., and Amin, A. Chinese Journal of Physics 56(4), 1481-1487 (2018); https://doi.org/10.1016/j.cjph.2018.06.003.
[10] B. Bouadjemi, S. Bentata, A. Abbad, and W. Benstaali, Solid State Commun. 207 9–15 (2015); https://doi.org/10.1016/j.ssc.2015.02.001
[11] Fukuda, M., Yamada, I., Murata, H., Hojo, H., Hernandez, O. J., Ritter, C., Tanaka, K., Fujita, K. Chemistry of Materials 32(12), 5016-5027 (2020); https://doi.org/10.1021/acs.chemmater.0c00444.
[12] Yu, R., Hojo, H., Mizoguchi, T., and Azuma, M. Journal of Applied Physics 118(9), 094103 (2015); https://doi.org/10.1063/1.4930034.
[13] Astudillo, J. A., Dionizio, S. A., Izquierdo, J. L., Morán, O., Heiras, J., and Bolaños, G. AIP Advances 8(5), 055817 (2018); https://doi.org/10.1063/1.5007783.
[14] Liang, Y., and Shao, G. RSC Advances 9(13), 7551-7559 (2019); https://doi.org/10.1039/C9RA00289H
[15] Yaseen, M., Aldaghfag, S. A., and Zahid, M. Materials Science in Semiconductor Processing 147, 106760 (2022); https://doi.org/10.1016/j.mssp.2022.106760.
[16] Azam, S., Irfan, M., Abbas, Z., Rani, M., Saleem, T., Younus, A., Akhtar, N., Liaqat, B., Shabbir, M., and Al-Sehemi, A. G. Digest Journal of Nanomaterials and Biostructures 14(3), 751-760 (2019);
[17] Zhang, T., Wu, Q., Wu, X., Gu, Y., Gao, Z. P., Nie, H. C., Li, J., and Deng, M. H. Journal of Alloys and Compounds 778, 787-794 (2019); https://doi.org/10.1016/j.jallcom.2018.11.119.
[18] Song, B., Wang, X., Xin, C., Zhang, L., Song, B., Zhang, Y., Wang, Y., Wang, J., Liu, Z., Sui, Y., and Tang, J. Journal of Alloys and Compounds 703, 67-72 (2017); https://doi.org/10.1016/j.jallcom.2017.01.180.
[19] Okoye, C. M. I. Journal of Physics: Condensed Matter 15(35), 5945 (2003); https://doi.org/10.1088/0953-8984/15/35/304
[20] Wang, Q., Han, Y., Liu, C., Ma, Y., Ren, W., and Gao, C. Applied Physics Letters 100(17), 172905 (2012); https://doi.org/10.1063/1.4706255.
[21] Zhang, X., Li, G., Mao, F., Han, D., Jing, C., Chen, Y., Yang, P., Chu, J., and Yue, F. Ceramics International 46(11), 18026-18031 (2020); https://doi.org/10.1016/j.ceramint.2020.04.118.
[22] Shen, Y., and Zhou, Z. Chemical Physics Letters 454(1-3), 114-117 (2008); https://doi.org/10.1016/j.cplett.2008.01.079.
[23] Naz, A., Aldaghfag, S. A., Yaseen, M., Butt, M. K., Kashif, M., Zahid, M., Mubashir, S., and Somaily, H. H. Physica B: Condensed Matter 631, 413714 (2022); https://doi.org/10.1016/j.physb.2022.413714.
[24] H. Shafique , S. A. Aldaghfag , M. Kashif , M. Zahid, M. Yaseen , J. Iqbal , R. Neffati, Chalcogenide Letters, **18**(10), 589 - 599 (2021); https://doi.org/10.15251/CL.2021.1810.589
[25] Yaseen, M., Butt, M. K., Ashfaq, A., Iqbal, J., Almoneef, M. M., Iqbal, M., Murtaza, A., and Laref, A. Journal of Materials Research and Technology 11, 2016-2113 (2021); https://doi.org/10.1016/j.jmrt.2021.02.017.
[26] Yaseen, M., Ambreen, H., Zia, M., Javed, H. A., Mahmood, A., and Murtaza, A. Journal of Superconductivity and Novel Magnetism 34(1), 135-141 (2021); https://doi.org/10.1007/s10948-020-05674-0
[27] Yaseen, M., Dilawar, M., Ambreen, H., Bibi, S., Rehman, S. U., Shahid, U., Butt, M. K., Ghaffar, A., and Murtaza, A. Bulletin of Materials Science 43(1), 1-8 (2020); https://doi.org/10.1007/s12034-020-2078-8
[28] Luo, B., Wang, X., Tian, E., Li, G., and Li, L. Applied Surface Science 351, 558-564 (2015); https://doi.org/10.1016/j.apsusc.2015.05.140.
[29] Yaseen, M., Ambreen, H., Iqbal, J., Shahzad, A., Zahid, R., Kattan, N. A., Ramay, S. M., and Mahmood, A. Philosophical Magazine 100(24), 3125-3140 (2020); https://doi.org/10.1080/14786435.2020.1812748.

[30] Mahmood, Q., Haq, B. U., Yaseen, M., Ramay, S. M., Ashiq, M. G. B., and Mahmood, A. Solid State Communications 292, 17-23 (2019); https://doi.org/10.1016/j.ssc.2019.01.011.
[31] Gagui, S., Zaidi, B., Megdoud, Y., Hadjoudja, B., Chouial, B., Meradji, H., Ghemid, S., and Shekhar, C., Computational Condensed Matter 22, e00433 (2020); https://doi.org/10.1016/j.cocom.2019.e00433
[32] Bilal, M., Khan, B., Aliabad, H. R., Maqbool, M., Asadabadi, S. J., and Ahmad, I. Computer Physics Communications, 185(5), 1394-1398 (2014); https://doi.org/10.1016/j.cpc.2014.02.001.
[33] Sarfraz, S., Aldaghfag, S. A., Butt, M. K., Yaseen, M., Zahid, M., and Dahshan, A. Materials Science in Semiconductor Processing 148, 106811 (2022); https://doi.org/10.1016/j.mssp.2022.106811.
[34] Golovina, I. S., Shanina, B. D., Kolesnik, S. P., Geifman, I. N., and Andriiko, A. A. Journal of Applied Physics 114(17), 174106 (2013); https://doi.org/10.1063/1.4829702.
[35] Saleem, S., Aldaghfag, S. A., Yaseen, M., Butt, M. K., Zahid, M., Murtaza, A., and Laref, A. The European Physical Journal Plus 137(1), 121 (2022); https://doi.org/10.1140/epjp/s13360-022-02352-z